Indian Journal of Engineering & Materials Sciences
Vol. 33, June 2026, pp. 324-343
DOI: 10.56042/ijems.v33i03.25032

Flexural and hardness performance prediction of hybrid composites via machine learning and experimental validation

Jothi Arunachalam Solairaju[a], Saravanan Rathinasamy[a], Vinuja Gurumoorthy[b], Sathish Thanikodi[a*] & AndersonArul Gnana Dhas[c]

[a]Department of Mechanical Engineering, Saveetha School of Engineering, Saveetha Institute of Medical and Technical Sciences, Chennai 602 105, Tamil Nadu, India

[b]Department of Computer Science and Engineering, Veltech Rangarajan Dr.Sagunthala R&D Institute of Science and Technology, Chennai 600 062, Tamil Nadu, India

[c]Department of Aeronautical Engineering, Sathyabama Institute of Science and Technology, Chennai 600 119, Tamil Nadu, India

Received 24 October2025: ; accepted:05 March 2026

This study has investigated the flexural strength and hardness of a hybrid composite reinforced with jute, kenaf, and glass fibers and filled with aluminium oxide (Al_2O_3) nanoparticles. The mechanical performance of the composites with (1) different fiber orientations (0°, 45°, and 90°), (2) different stacking sequences (1–3 layers), and (3) different Al_2O_3 contents (3–5 wt%) has been systematically evaluated. Response surface methodology (RSM) has been utilized to determine parameter interactions and statistical significance and to optimize the experimental conditions. Artificial neural networks (ANN), generative adversarial networks (GAN), and feed-forward neural networks (FFNN) have been employed for predictive modelling. Among these approaches, FFNN has demonstrated the highest prediction accuracy, closely matching the experimental results and outperforming GAN and RSM. The optimal combination of parameters has been identified as a 90° fiber orientation, 5 wt% Al_2O_3 content, and the stacking sequence G/J/J/K/K/K/K/J/J/G, which has enhanced the flexural strength by 18% and hardness by 32%. The effective predictive capability of FFNN has been confirmed by the lowest prediction errors, with a Mean Absolute Error (MAE) of 15.05 and a mean squared error (MSE) of 47.65, demonstrating that FFNN has provided superior predictive performance.

Keywords: Hybrid composites, Nanoparticles, Natural resources, Optimization, Predictive modelling, Synthetic fibers

1 Introduction

In recent years, there has been a growing interest in utilizing natural resources-based fibers as reinforcement materials for composites due to their lightweight nature, cost-effectiveness, ease of processing, and environmental benefits (Raj[1]; Raja[2]). Natural resources-based fiber composites are key to promoting sustainable development and are well-suited for various applications, including aerospace, sports equipment, and automotive components, such as dashboards, for sustainable use(Solairaju[3]; Velmurugan[4]; Thanikodi[5]). Nanoparticles often result in a significant bonding agent between fiber and matrix (Sekhar[6]). However, natural resources-based fibers often exhibit limited interfacial adhesion and high moisture absorption, making them hygroscopic, which can lead to fiber swelling, micro-cracking, and degradation of mechanical properties in composites(Pradeep[7]). To address these challenges, chemical treatments are applied to fibers to reduce moisture absorption, improve chemical composition (such as cellulose, hemicellulose, and lignin), enhance tensile strength and elongation, reduce shrinkage, and increase compatibility between the fiber and matrix(Lakshmaiya[8]) This treatment also chemically alters surface roughness by reducing the hydroxyl groups involved in hydrogen bonding within cellulose molecules, further improving fiber performance in composites(Xian[9]).

The neural network's projected values closely align with the actual values, with a variance of merely ten percentage. The ANN predictions were compared with an establish RSM model. The Experimental results demonstrate that concrete reinforced with 0.5% bamboo fibers, 0.5% jute fibers, and 10% silica fume (SF) markedly improved its mechanical qualities. The suggested ANN model shown a significant level of accuracy in predicting the

*Corresponding author (E-mail: sathisht.sse@saveetha.com)

mechanical characteristics of natural-fiber-reinforced concrete (Aisheh[10]).

Natural resources-based fiber composites were created with bamboo fibers bonded with nano-silica within an epoxy resin matrix. The composites were investigated by combining an appropriate quantity of nano-SiO_2 with bamboo fibers, and the impacts of bamboo fiber and nano-silica were evaluated using Analysis of Variance (ANOVA). Experimental findings demonstrated that a design including two layers of bamboo fiber and 2 wt.% nano-silica yielded a superior composite. Bamboo fiber-reinforced nanocomposites possess a wide range of applications in the aerospace, auto, athletic equipment, structural, and household appliance sectors (Shah[11]).An artificial neural network model was utilized to forecast the attributes of the fiberboard and was later implemented as the function of fitness in an optimization with multiple objectives of the fiberboard using the NSGA-II method. A comparison methodology was established, employing a conventional multi-objective optimization tool, the desirability function, alongside a Response Surface Methodology (RSM) model. The optimized Pareto front generated by the NSGA-II algorithm provided a significant design reference for the actual uses of the composite (Liu[12]).In comparison to other composites, the fiber-oriented Composite A demonstrated the highest interlaminar shear strength (ILSS) of 3.35 MPa. The ANN model precisely forecasted strength values, with elevated R^2 scores of 1 for mechanical properties. The correlation coefficients in the framework were approximately 1, indicating a robust association and elevated prediction accuracy (Sridhar[13]).

The constructed model demonstrated robust concordance with experimental results, signifying high prediction accuracy. The incorporation of sugarcane bagasse and alumina micro-fillers into the epoxy resin markedly enhanced the mechanical characteristics. hybrid composite validated the uniform distribution of sugarcane bagasse and aluminum oxide particles within the epoxy matrix, which enhances the product's mechanical characteristics (Senthilkumar[14]).Various quantities of fiber and filler material were synthesized using an L25 orthogonal array to assess their mechanical qualities. A regression calculation was created for each mechanical characteristic utilizing RSM, articulated about fiber and filler weight. Statistical models were developed utilizing both RSM and ANN, and their prediction efficacy was evaluated through R^2 values. The R^2 results indicated that the ANN model surpassed the RSM model in predicting accuracy for this investigation (Nwobi-Okoye[15]).A tensile strength (TS) study was performed at the anticipated ideal settings to verify the dependability of the empirical inquiry. The TS results indicated an average of 45.44 MPa, with the model representing roughly 98.45% of the anticipated tensile strength. This study illustrates the efficacy of the ANN-BBD modeling approach in effectively attaining targeted mechanical property values, minimizing production costs, and preserving resources (Ramesh[16]). The regression models from Design Expert 13 facilitate the comprehension of the correlations between process factors and outcomes. Optimized input parameters provide methods to decrease surface roughness and kerf angle while enhancing material removal rate. This holistic methodology, integrating sophisticated machine learning and ensemble techniques, enhances predictive precision for banana composite materials and provides an adaptable structure for diverse materials handling applications (Arpitha[17]).

The integration of aluminum oxide fillers leads to the development of hybrid composites with superior mechanical properties compared to those containing a single type of filler. Aluminum oxide nanoparticles contribute to this enhancement by improving the hydrophobic interactions between the filler and the polymer matrix. This research focuses on composites reinforced with natural resources like jute and kenaf fibers, combined with synthetic glass fibers, and further modified with aluminum oxide nanoparticles. Designed for potential use in structural components within the automotive and aerospace sectors, these composites are analyzed using Artificial Neural Networks (ANN) to model the relationships between mechanical performance and filler characteristics. ANN-generated performance curves and regression analyses are employed to determine the optimal hybrid composite formulation, thereby enhancing material performance. The study specifically explores the effects of fiber orientation, fiber stacking sequence, and nanoparticle concentration on both flexural strength and hardness. Additionally, it examines the interactions among these variables during the composite fabrication process. To further refine the mechanical performance, Response Surface Methodology (RSM) is used to optimize critical processing parameters and evaluate their combined effects, with the ultimate goal of determining the most effective configuration of fiber alignment, stacking

order, and nano-filler content.This study introduces a novel approach by integrating Feed-Forward Neural Networks (FFNN) and Generative Adversarial Networks (GANs) to model and predict the mechanical behaviour of hybrid composites reinforced with jute, kenaf, and glass fibers, along with Al_2O_3 nanoparticles. While traditional modeling techniques like RSM and basic ANN have been widely used, this research distinguishes itself by employing GANs to augment limited experimental data and FFNN for enhanced predictive performance. The hybrid use of these advanced AI tools demonstrates improved accuracy in forecasting flexural strength and hardness, offering a more robust framework for optimizing composite design in structural applications.

2 Materials and Methods

Fiber-reinforced polymer composites are produced through an intricate process that starts with the careful selection of materials. For this composite, unidirectional woven natural resource Jute/kenaf fiber and glass fiber with a weight of 360 grams per square meter (GSM) was chosen. Epoxy LY556 was selected as the bonding agent due to its excellent adhesive properties, mechanical strength, and chemical resistance(Ramakrishnan[18]). To further enhance these characteristics, Al_2O_3, supplied by Ad-Nano Technology Pvt Ltd in Shivamogga, India, was incorporated. Jute and kenaf fibers were sourced from Hayael Aerospace Pvt Ltd in Chennai, India, while glass fiber, epoxy LY556, and hardener HY951 were obtained from Javanthee Enterprises, also located in Chennai. The production process is a detailed procedure that starts with the careful selection of appropriate materials.

2.1 Composite preparation

Laminated composite specimens measuring 300 × 300 × 4 mm were fabricated with varying amounts of Al_2O_3filler (3, 4, and 5 g) incorporated into jute/kenaf/glass composite. The composites were prepared using three different fiber sequences: Sequence 1 (G/K/K/K/K/J/J/J/J/G), Sequence 2 (G/K/K/J/J/J/J/K/K/G), and Sequence 3 (G/J/J/K/K/K/K/J/J/G). These predefined sequences were designed to evaluate the effect of fiber positioning on mechanical performance. The order was strictly followed during fabrication, with each layer manually placed according to the assigned stacking sequence. By controlling the fiber order, we could systematically study the influence of inner and outer fiber layers on flexural strength and hardness. The fabrication process involved hand lay-up followed by compression molding. The jute, kenaf, and glass fabrics were cut and arranged as specified, and epoxy LY556 mixed with hardener HY951 in a 10:1 weight ratio was applied. Each composite maintained a uniform matrix ratio of 40% by weight(Imoisili[19]). Epoxy was applied to the fabric surfaces, then compression molded at 80°C with a pressure of 5 kg cm^{-2} for one day. After molding, the laminated composites were removed from the steel die and left to cure for an additional 24 hours at room temperature. The composite panels were then cut using an ASTM-compliant water jet machine (WJM) to test hardness and flexural strength (FS). Following the WJM process, the specimens were post-cured in a heated air oven at 60°C for 4 hours to eliminate any residual moisture.

2.2 Design of experiments

RSM is a powerful technique used to analyze and optimize systems affected by multiple factors that influence the desired outcome. It integrates various statistical and mathematical approaches, offering advantages over traditional factorial methods. The Central Composite Design (CCD) is one of the most widely used RSM strategies. This technique requires a minimum number of N trials to develop a mathematical model for "f" variables. The study focused on the FS and hardness of an epoxy composite reinforced with jute, kenaf, and glass fibers, with Al_2O_3used as a filler(Saravanakuma[20]). The independent variables investigated included the weight percentage of Al_2O_3 filler, fiber sequence, and fiber orientation in degrees. Table 1 lists the input low and high values for these parameters, while Table 2 presents 20 samples with various combinations of the three components. All possible permutations were tested in a randomized order to minimize errors. Additionally, Fig. 1(a) illustrates the samples during loading, and Fig. 1(b) shows the sample after the test.

3 Results and Discussion

3.1 Data-driven evaluation for FS

The Flexural test analysis is done using ‘Design Expert 13’ software after the formulation of a Central Composite Design (CCD). Table 2 presents the factors and the expected outcome of each. The initial models were formed from the primary input data and

Table 1 — Input factors and levels.

	Name	Units	Low	High
A	Fiber orientation	Degree	0	90
B	Fiber sequence		1	3
C	Al_2O_3 Filler	%	3	5

Table 2 — Input factors and output responses from RSM.

Std	Run	A: Fibre orientation (FO)	B: Fibre sequence (FSS)	C: Filler	Flexural Strength	Hardness
		Degree		%	MPa	HRC
3	1	0	3	3	114	66
12	2	45	3	4	127	80
4	3	90	3	3	128	79
19	4	45	2	4	121	74
9	5	0	2	4	115	68
2	6	90	1	3	123	75
11	7	45	1	4	120	73
1	8	0	1	3	109	62
8	9	90	3	5	131	83
5	10	0	1	5	112	65
14	11	45	2	5	125	78
18	12	45	2	4	122	75
20	13	45	2	4	124	77
16	14	45	2	4	122	74
10	15	90	2	4	126	78
13	16	45	2	3	119	71
7	17	0	3	5	118	70
6	18	90	1	5	126	78
17	19	45	2	4	123	75
15	20	45	2	4	123	75

produced a second-order polynomial type of model, which indicated key model terms that followed A, B, C, and A^2. There were analyzed Linear regression models of outcomes concerning coded variables were analysed according to formula (1).

$$FS = 90.396 + 0.266 \times A - 0.302 \times B + 8.320 \times C - 0.003 \times A - 0.003 \times AC + 0.125 \times BC - 0.001 \times A^2 + 0.682 \times B^2 - 0.818 \times C^2 \quad ...(1)$$

In this analysis, coded variables shown as A -FO, B – FSS, and C - Al_2O_3 weight percentage were used to estimate FS using the quadratic equation. The research provides statistical parameters like mean square (MS) and sum of squares (SS) in Table 3. The calculated F-value of 48.83 also shows statistical significance because there is only a 0.01% chance that such an F-value is due to noise. Modeling terms with P-values less than 0.0500 were considered to be of significant importance, while terms with P-values higher than 0.1000 were deemed insignificant. To improve the efficiency of the model, attempts should be made to

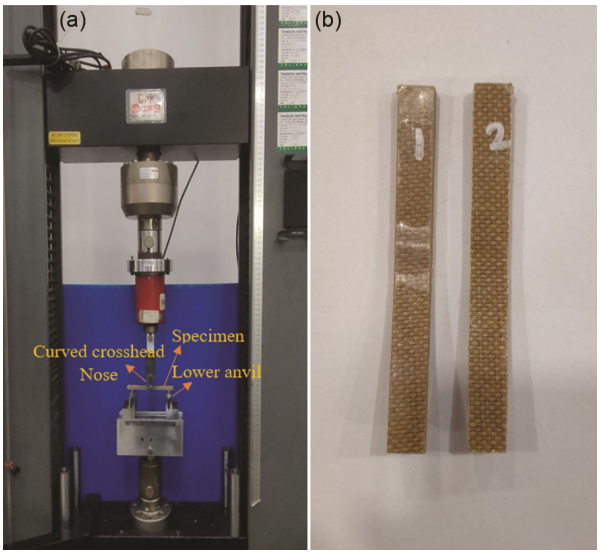


Fig.1 — Flexural test (a) During loading and (b) After the tested sample.

reduce the number of terms. The statistically analyzed R^2 corrected to 0.9778 indicates a very high degree of common variation between the two sets; an Adeq Precision ratio of > 4 suggests an adequate distinction between the signal and noise. Also, the Lack of Fit (LOF) F-value of 7.73 approved the probability of this level of error from random noise is only 0.01%.

Figure 2 illustrates the correlation between the standard probability distribution and the internal residual FS. As it is evident from Fig. 2(a), the residual points are close to the curve, and this explanation reads that the data fit is good. Again, if we examine the residuals, they depict little variations from the normal distribution pattern. Figure 2(b) revealed the scatter plot of the experimental and residual FS values, and all the points were close to the zero cross, suggesting a relatively stable variation and, therefore, no need for data transformation. The trends in the dispersions for FS values are shown in Fig. 2(c) by the scatter plot of observed and predicted FS values. The scatter points are uniformly distributed along the axis in Fig. 2(d) and indicate a good agreement between the experimental and predicted values. It is evident from Fig. 2(d) that all the data points are approaching the reference line, proving that the model is very accurate. (Arunachalam[21]) used a response surface approach to optimize Jute/Kenaf/glass fiber composites and SiO_2 filler, and their findings are consistent with this discovery.

The perturbation plot, which analyzes the dependency of the FS response on each process

Table 3 — ANOVA for FS.

Factor	SS	df	MS	F-value	p-value	SS
Model	581.57	9	64.62	48.83	< 0.0001	significant
A-FO	435.60	1	435.60	329.15	< 0.0001	
B-FSS	78.40	1	78.40	59.24	< 0.0001	
C-Al_2O_3	36.10	1	36.10	27.28	0.0004	
AB	0.1250	1	0.1250	0.0945	0.7649	
AC	0.1250	1	0.1250	0.0945	0.7649	
BC	0.1250	1	0.1250	0.0945	0.7649	
A^2	14.78	1	14.78	11.17	0.0075	
B^2	1.28	1	1.28	0.9660	0.3489	
C^2	1.84	1	1.84	1.39	0.2655	
Residual	13.23	10	1.32			
Lack of Fit	7.73	5	1.55	1.41	0.3587	not significant

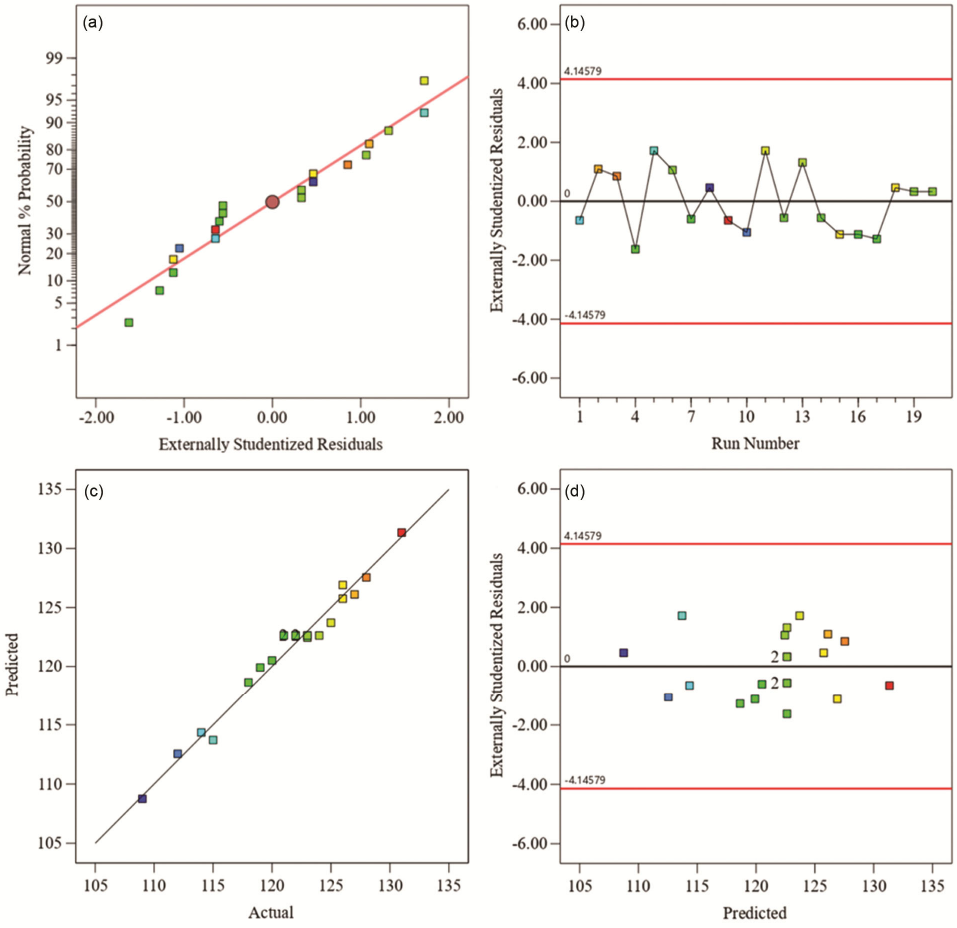


Fig. 2 — Flexuralresponse plot (a) Normal plot, (b) Residual versus Run number, (c) Predicted versus Actual and (d) Predicted versis Externally studentized residuals.

variable, is presented in Fig. 3. This plot shows how a single factor affects the response when the other factors are held constant, as well as evaluating the effect of each factor using the mid and zero-coded levels. Al_2O_3 content (C) is found to improve the FS when increased, probably due to increased toughness and better adhesion with the epoxy matrix. Likewise, FS rises with an enhancement of the degree of FO (A) due to its capacity to bear loads. On the other hand, FS is inversely proportional to FSS (B), attributed to a decrease in FO and interfacial adhesion between the fibers and the polymer matrix.

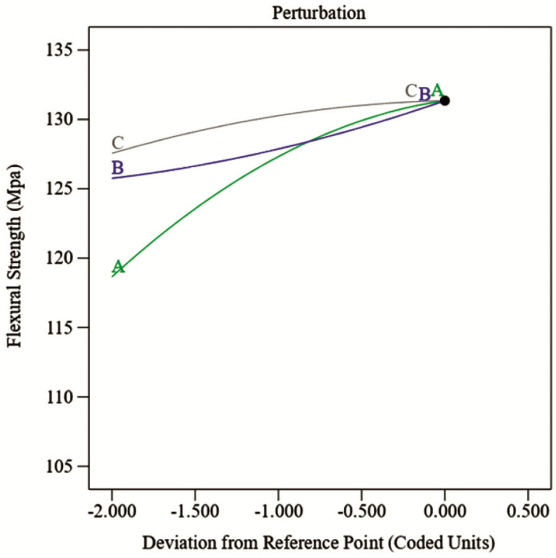


Fig. 3 — Perturbation plot for FS.

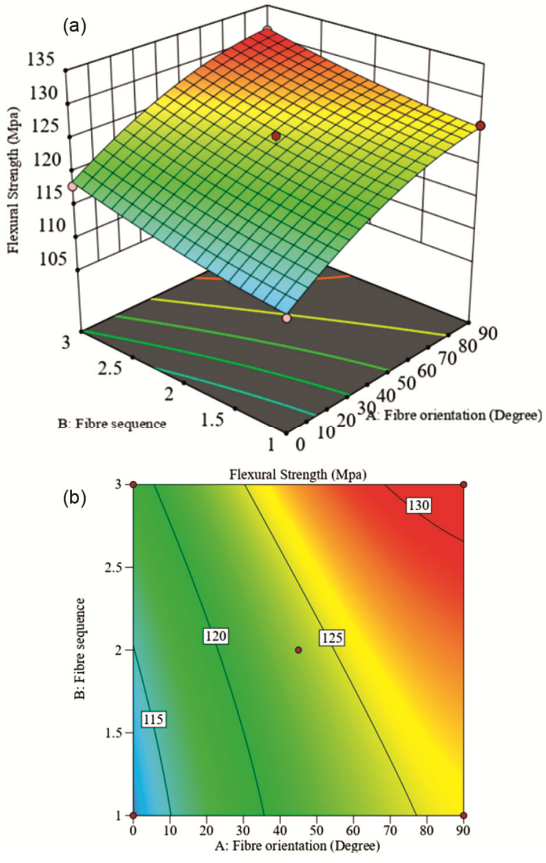


Fig. 4 — AB interaction for FS (a) 3D plot and (b)2D plot.

3.2 Surface response for FS

Figure 4 shows the three-dimensional surface plots and two-dimensional contour maps of FS in terms of different factors. Fig 4(a &b) show that FO and fiber sequencing affect FS. FO diagrams show that FS is substantially improved by the alignment of the fibers, but there is a decrease when orientation and arrangement are changed. Maximum FS occurs at a fiber orientation of 90 degrees and when the fiber is placed in a sequence of 3. This relative shift in the orientation of the fibers is illustrated from the 3D plot in Fig. 4(a), which shows how FS decreases for the FO as it moves away from the fiber sequence. Likewise, the 2D contour plot represented in Fig. 4(b) also supports this, with the FS reaching its maximum at 5 wt% of Al_2O_3 and minimum at 3 wt%. For this purpose, Fig. 5(a) shows the 3D surface plot, and Fig. 5(b) shows the 2D contour plot of the FS concerning Al_2O_3 concentration and FO. According to this analysis, using 5% Al_2O_3 increases FS but further rises to 4 wt% reduce FS due to poor load distribution within the laminated composite.

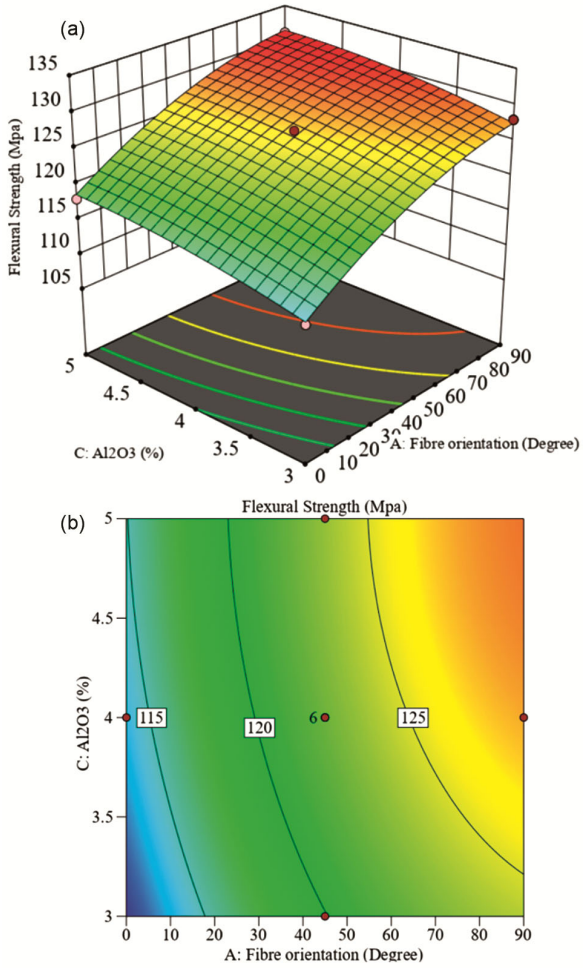


Fig. 5 — AC interaction for Flexural strength (a) 3D plot and (b)2D plot.

Figure 6(a &b) are the 3D and 2D plots that explain the interactive influence of fiber sequencing and

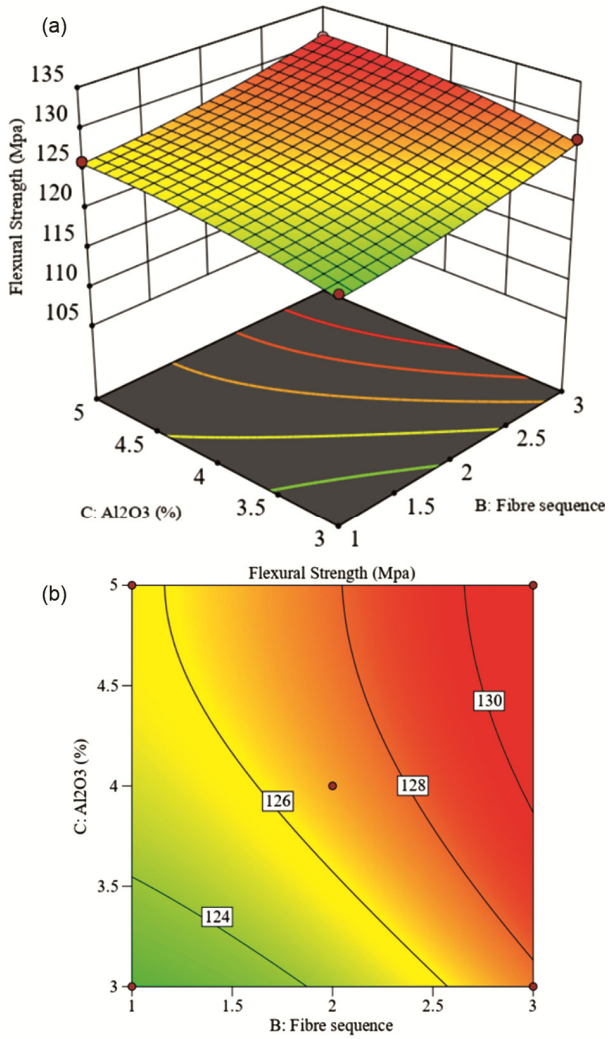


Fig. 6 — BC interaction for Flexural strength (a) 3D plot and (b)2D plot.

Al_2O_3 concentration on FS in the hybrid composite. Based on the 3D surface plot, when raising the Al_2O_3 concentration to as high as 5%, FS improves, which the authors attributed to better dispersion and reduced nanoparticle clustering in the matrix. Moreover, FS increases when using Al_2O_3 and optimizing the fiber placement as the bonding between the hybrid fibers and the epoxy resin is enhanced. These findings align with the results of (Nugroho[22]), who demonstrated that a 90-degree FO offers superior FS.

3.3 Statistical analysis of H

This work adopted Design Expert 13 software with an H test and CCD design. About the results of the multiple regression analysis of the initial data, the use of the second-order polynomial equation was employed. The values of the model's terms were found to be A, B, C, and A^2. The last solution was obtained using the formula shown in equation (2).

Table 4 — ANOVA for H.

Factors	SS	df	MS	F-value	p-value	
Model	534.86	9	59.43	32.41	< 0.0001	significant
A-FO	384.40	1	384.40	209.64	< 0.0001	
B-FSS	62.50	1	62.50	34.09	0.0002	
C-Al2O3	44.10	1	44.10	24.05	0.0006	
AB	0.0000	1	0.0000	0.0000	1.0000	
AC	0.0000	1	0.0000	0.0000	1.0000	
BC	0.5000	1	0.5000	0.2727	0.6129	
A^2	19.11	1	19.11	10.42	0.0090	
B^2	2.05	1	2.05	1.12	0.3151	
C^2	3.55	1	3.55	1.94	0.1942	
Residual	18.34	10	1.83			
Lack of Fit	12.34	5	2.47	2.06	0.2239	not significant

$$H = 40.291 + 0.255 \times A - 1.955 \times B + 10.691 \times C + 2.099e^{-16} \times AB + 1.885e^{-16} \times AC + 0.25 \times BC - 0.001 \times A^2 + 0.864 \times B^2 - 1.136 \times C^2 \quad \ldots(2)$$

The multiple linear regression model with coded variables. These coded variables,FO (A), FSS (B), and Al_2O_3 weight percentage (C), were used in a quadratic model to predict the effect of each factor. In Table 4, the ANOVA analysis compares the amount of variation between groups MS to that within the groups (MS error) and derives an F-ratio and a P-value, which comprises parameters such as MS and the sum SS. The model was significant, with an F-value of 32.41, which was relatively small compared with the probability of such a large value arising from random fluctuation, given at least 0.01%. Model terms significant in defining a P-value of less than 0.0500 include A, B, C, and A^2, while non-significant model terms worthy of removal due to their inefficiency include terms defining a P-value of more than 0.1000. The Adjusted R^2 value of 0.9669 pointed out the strength of the model between the predicting and the actual data, and the Adequate Precision ratio supported the model's good signal-to-noise ratio. The F-statistic for LOF of 12.34 indicates the significance of the model and the probability of such an error due to noise being 0.01%. In this evaluation, pure error was compared to the residual error from replicate design values to determine the appropriateness of the model for estimating data.

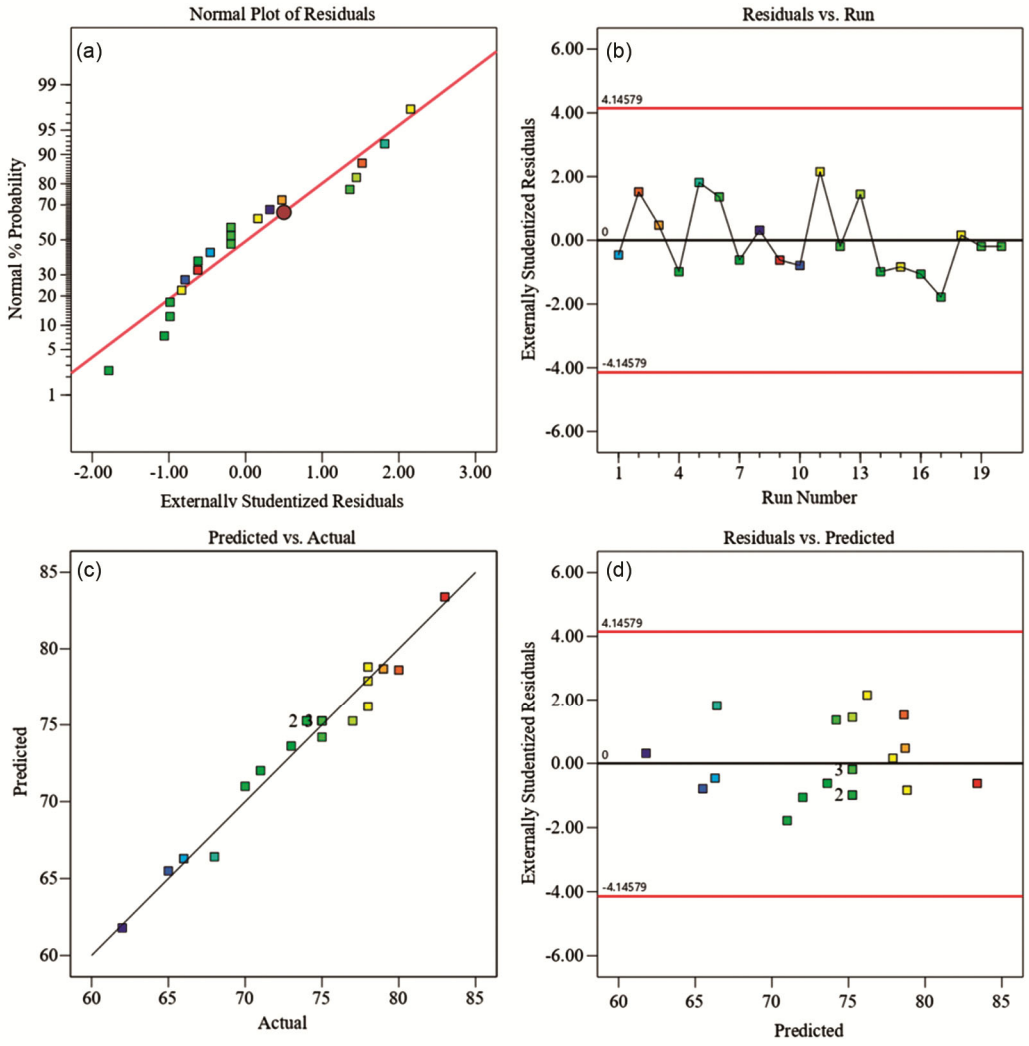


Fig. 7 — Hardness response plot (a) Normal plot, (b) Residual versus Run number, (c) Predicted versus Actual and (d) Predicted vs Externally studentized residuals.

A comparison of the standard probability distribution and internal residuals for hardness is shown in Fig. 7(a–d). Similar to Fig. 5(a), the residual plot also fits the normal distribution with no signs of violation of the normality assumption, as evidenced by most of the residual points hugging the curve in Fig. 7(a). In Fig. 7(b), the experimental values of H are plotted against the residuals, and the points are scattered around the zero line. Stability in variance also indicates the appropriateness of no further data transformation. Figure 7(c) shows the actual and predicted H values, where the scatter of the point indicates the difference between the findings from the expected outcome. Figure 7(d) illustrates scatter points aligned with the axis and, thus, points to a direct correspondence between experiment and predictions. As targets focus on the line of reference, the ability of the model to predict becomes better, as seen in Fig. 7d.

Figure 8 is a conventional perturbation plot showing the extent to which each process variable influences the H response. From the plot, it can be inferred that as the content of Al_2O_3 (C) increases, so does H. The sample probably enjoys the benefits of a tough and strongly bonded Al_2O_3/epoxy matrix. It increases with FO (A) because such orientations enhance load-carrying capacity. On the other hand, H is inversely proportional to FSS (B) because of increasing fiber arrangement and poor interfacial adhesion of the fibers-polymer matrix. The finding aligns with the earlier work conducted by (Niyaraki[23]).

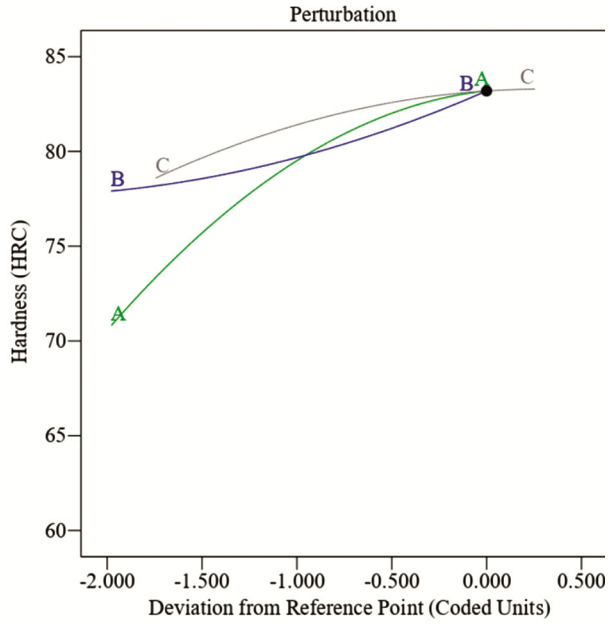


Fig. 8 — Perturbation plot for hardness.

3.4 Surface response for H

Figure 9 shows the three and two-dimensional graphs representing H depending on various factors. Figure 9(a &b) depict how FO as well as FSS affect H. Based on these analyses of FO plotted against the 3D surface, it can be concluded that FO plays a key role in the enhancement of H with near-optimal values of the parameter. Nonetheless, a decrease in H is achieved when both FO and arrangement change; the maximum H is at FO 90° and sequence 3. Furthermore, Fig.9(a) shows a 3D plot where H is reduced as the orientation changes compared to the fiber sequence. Figure 9(b) is the 2D contour plot ofH of the toughened composites, in which H increases to a maximum in 5 wt % Al_2O_3 and decreases to the a minimum value at 3 wt %(Arunachalam[24]). In the 3D surface plot and the 2D contour plot obtained in Fig. 10(a &b), the interaction between Al_2O_3 concentration and FO on H is shown. In a 3D surface analysis, it is shown that H increases with Al_2O_3 concentration up to 5%, but a decrease is observed when the concentration is 5% for different FO. This decrease may be attributed to the fact that at this Al_2O_3 concentration, the laminated composite's load-bearing ability has been compromised. Actual 3D surface and 2D contour plots presented in Fig. 11(a &b) depict the impact of fiber sequence and Al_2O_3 concentration on H. The 3D plot analysis reveals that a higher Al_2O_3 concentration of 5% improves H, which may be attributed to improved distribution of Al_2O_3 and its existence as clusters of

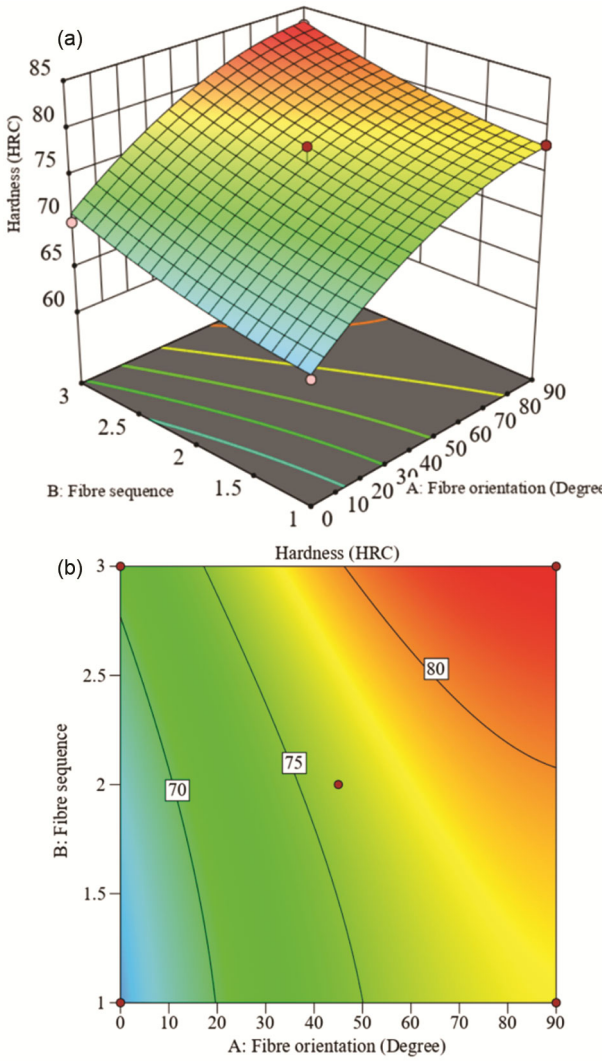


Fig. 9 — AB interaction for hardness (a) 3D plot and (b) 2D plot.

nanoparticles in the matrix. Moreover, it rises with an increase of Al_2O_3 modification and the varied fiber dispositions, which are probably attributed to enhanced connectivity between the fibers and the epoxy matrix (Arunachalam[25]).

The experimental data presented indicate a clear enhancement in the flexural strength and hardness of fiber-reinforced composites with increasing percentages of Al_2O_3 filler. Across various combinations of FO and FSS, a consistent trend is observed where samples containing higher Al_2O_3 content, particularly at 4% and 5%, demonstrate improved mechanical performance compared to those with lower filler levels (3%). For instance, with a fiber orientation of 90° and FSS of 3, increasing the Al_2O_3 filler from 3% to 5% resulted in a flexural strength increase from 128 MPa to 131 MPa and a corresponding rise in hardness from 79 HRC to

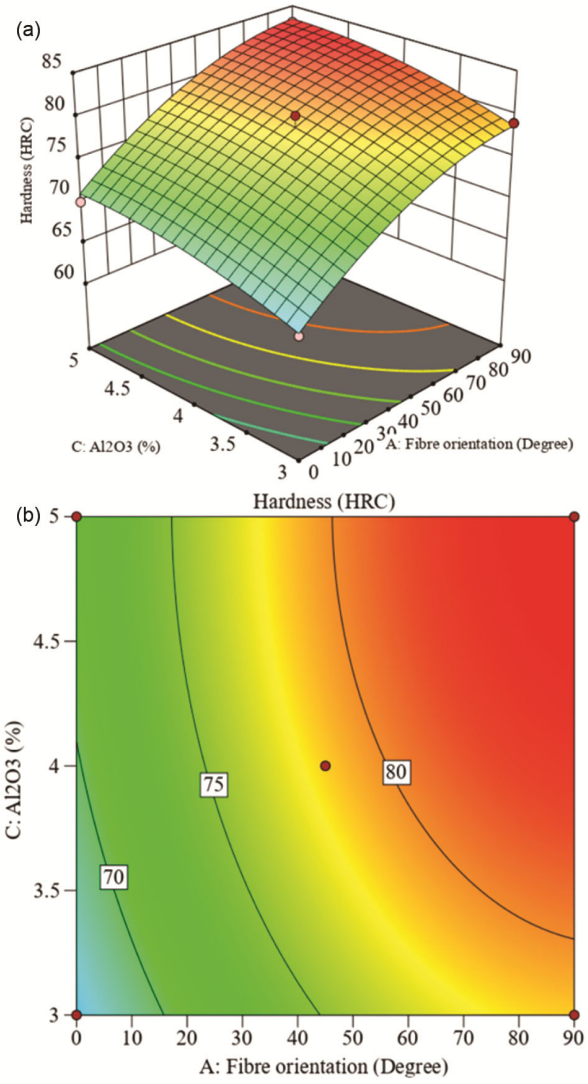


Fig. 10 — AC interaction for hardness (a) 3D plot and (b) 2D plot.

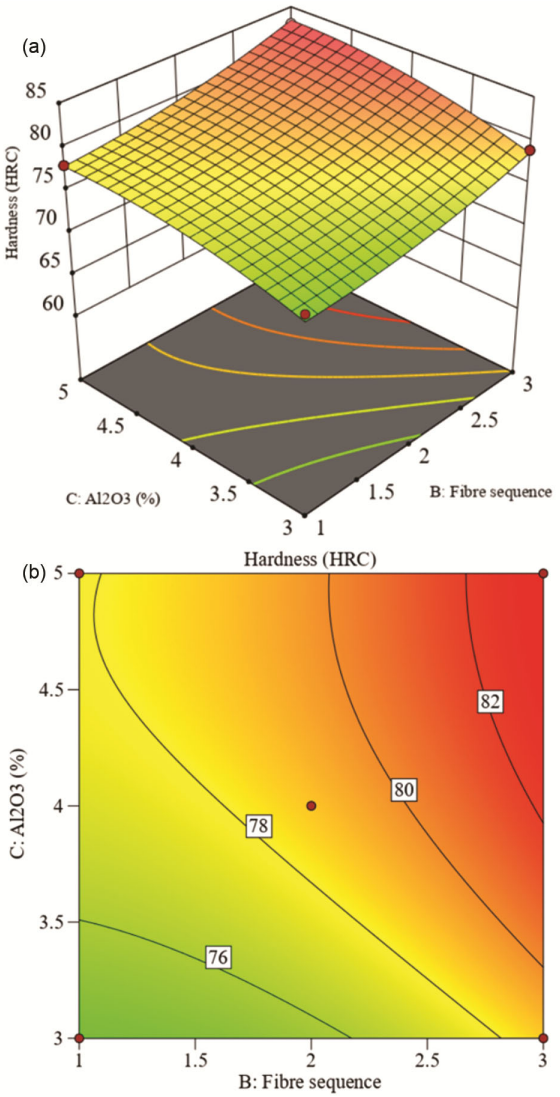


Fig. 11 — BC interaction for hardness (a) 3D plot and (b) 2D plot.

83 HRC. Similarly, at a 45° orientation with FSS = 2, a comparison between 4% and 5% filler shows strength rising from 122 MPa to 125 MPa and hardness from 75 HRC to 78 HRC. Even in samples with a fiber orientation of 0°, improvements are evident, such as an increase from 109 MPa to 112 MPa in flexural strength and from 62 HRC to 65 HRC in hardness when filler content rises from 3% to 5%.These enhancements can be attributed to the role of Al_2O_3 nanoparticles in improving the interfacial bonding between the fiber and matrix. The rigid ceramic nature of Al_2O_3 contributes to improved load transfer efficiency and resistance to deformation under bending and surface indentation. Overall, the incorporation of Al_2O_3 significantly improves the mechanical performance of the composites, with 5% filler content showing optimal results.

Table 5 presents statistical analysis for flexural strength and hardness measurements. For both properties, predicted mean and median values closely match the observed data, indicating good model accuracy. Flexural strength shows a predicted mean of 131.348 with an observed value of 131, while hardness has a predicted mean of 83.396 compared to an observed value of 83. Standard deviations are low, suggesting limited variability across the small sample size (n = 3). The standard errors of prediction (SE Pred) quantify uncertainty, while the 95% prediction intervals provide likely ranges for future observations, demonstrating reliability in both data sets with consistent mean comparisons.

Figure 12 displays an optimization summary confirming the statistical results in the provided table.

Table 5 — Confirmation with observed results.

Analysis	Predicted Mean	Predicted Median	Observed	Std Dev	n	SE Pred	95% PI low	Data Mean	95% PI high
Flexural Strength	131.348	131.348	131	1.1504	3	1.221	128.627	131	134.068
Hardness	83.3955	83.3955	83	1.35412	3	1.43723	80.1931	84	86.5978

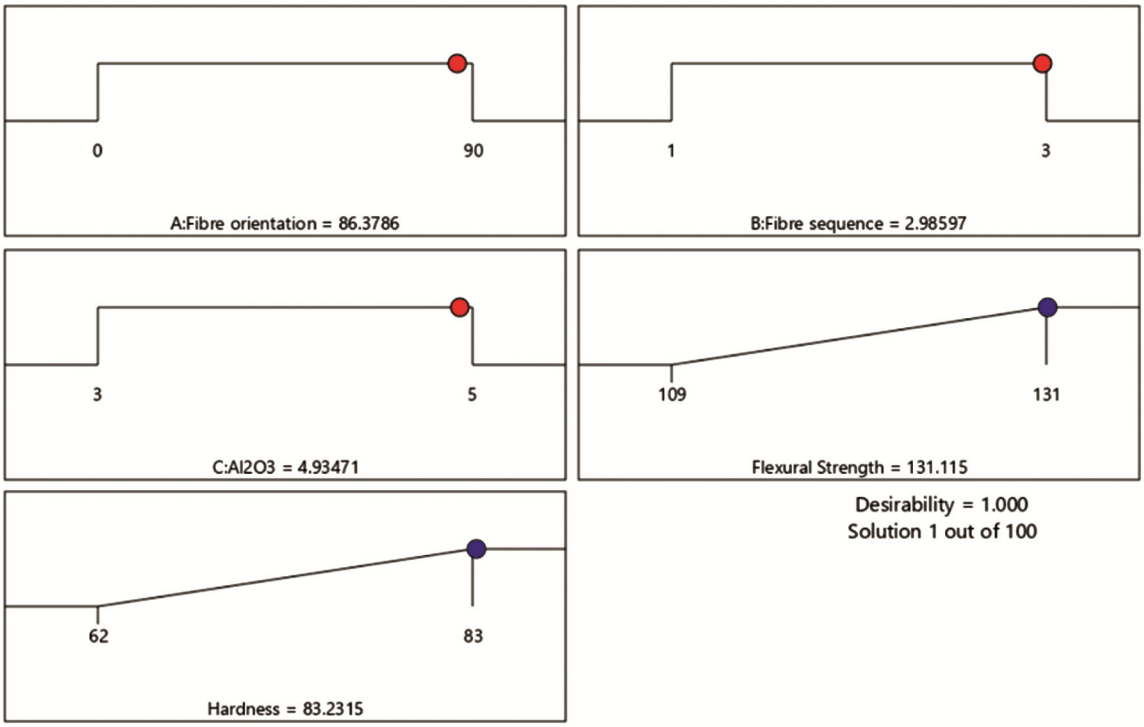


Fig. 12 — A Ramp plot confirming the statistical results in different aspects.

Each factorfibre orientation, fibre sequence, and Al_2O_3 contentis set near its optimal value, as indicated by the red dots on the upper ends of their ranges. The corresponding responses, flexural strength and hardness, reach their highest observed values (131.115 and 83.2315, respectively), matching those in the table. The desirability score of 1.000 signifies that the parameter settings fully satisfy the optimization criteria, supporting the table's confirmation of prediction accuracy and reliability. This alignment validates the chosen settings for maximum performance

3.5 Machine learning

ANNs are a type of current model of computation systems that are patterned after the brain and analyze data/information through tiered layers. It is made up of interconnected nodes, neurons that are grouped in input, hidden, and output layers. ANNs are trained from the data by periodically modifying parameters called connection weights, which then help the network recognize common patterns and make corresponding predictions in fields such as image recognition and optimization. The low chart machine learning (ML) shown in Fig. 13. ANNs called generational adversarial networks (GANs) were primarily created to perform generative tasks. They comprise two competing networks: a generator and a discriminator which were found to be significant in improving the general performance of the network (Feng[26]). The generator itself generates some samples of data and the discriminator judges whether or not they are real. This makes the generator better and as a result, GAN can be used in image synthesis, data augmentation, and in predictive modeling tasks.

A total of 20 experimental data points were generated using a full factorial design that incorporated three FO (0°, 45°, and 90°), three stacking sequences (1, 2, and 3 layers), and three Al_2O_3 weight percentages (3%, 4%, and 5%). To facilitate machine learning analysis, the dataset was randomly split into a training set comprising 70% of the data (14 samples) and a testing set containing the remaining 30% (6 samples). Pre-processing steps were carried out to prepare the data for modelling,

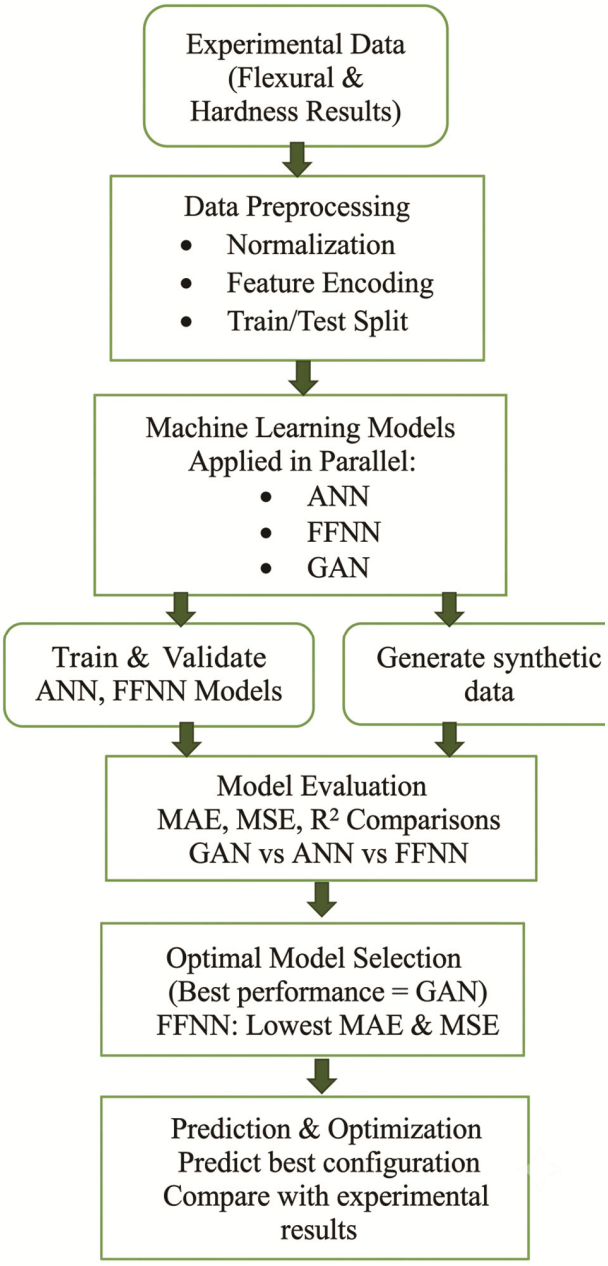


Fig. 13 — Flowchart for the ML workflow.

which included min-max normalization of all input and output variables to standardize their ranges and ensure consistent scaling during training. Additionally, categorical variables such as stacking sequences were numerically encoded to maintain compatibility with the machine learning algorithms. Given the limited size of the experimental dataset, Generative Adversarial Networks (GANs) were employed for data augmentation. The GANs generated synthetic data points that closely mimicked the statistical distribution of the original dataset. This augmentation process significantly enriched the training dataset, thereby enhancing the model's ability to generalize and improving the overall accuracy and robustness of the predictive outcomes.

3.5.1 Artificial Neural Network (ANN) – Flexural Strength

Inputs (standardized):

- AA = Fiber Orientation
- BB = Fiber Sequence
- CC = Filler (%)

Hidden Layer 1:

h1=max (0, −0.2874A−0.3339B+0.2257C+0.2535

h2=max (0,0.3269A+0.2365B−0.2652C+0.4193)

3.5.2 Feed-Forward Neural Network (FFNN) – Hardness

Inputs (standardized):

- A = Fiber Orientation
- B = Fiber Sequence
- C = Filler (%)

Hidden Layer 1:

h1=max (0, −0.2305A−0.3372B+0.2462C−0.0367))

h2=max (0,0.3099A+0.2400B−0.3131C+0.3441

Hidden Layer 2:

h3=max (0, −0.1734h1+0.1163h2−0.1172)

h4=max (0, −0.0058h2+0.1470)

Output Layer:

$Y_{hardness}$=−0.1316h3−0.1485h4+0.1761

3.6 Generative Adversarial Network (GAN)

The GAN generator model used for predicting flexural strength and hardness was a fully connected feed-forward neural network with two hidden layers using ReLU activation functions. The mapping from inputs (fiber orientation, fiber sequence, and filler percentage) to outputs (flexural strength and hardness) can be expressed as:

$$Y = W3 \times ReLU(W2 \times ReLU(W1 \times X + b1) + b2) + b3 \quad ...(3)$$

Where, X= [A, B, C] ^{T} and Y= [Y1, Y2] $^{T.}$

The architecture of the Feedforward Neural Network (FFNN) was carefully designed to predict dual output responses, flexural strength and hardness, based on three input parameters: FO, FSS, and Al_2O_3 weight percentage. The input layer consisted of 3 neurons corresponding to these variables. The network featured two hidden layers, with the first hidden layer containing 10 neurons and the second

hidden layer comprising 8 neurons. Both hidden layers employed the ReLU (Rectified Linear Unit) activation function to introduce non-linearity and enhance learning capability. The output layer consisted of 2 neurons, which simultaneously predicted flexural strength and hardness, utilizing a linear activation function suitable for regression tasks. For training, the Adam optimizer was utilized along with the Mean Squared Error (MSE) as the loss function. The model was trained over 500 epochs with a batch size of 4, and early stopping was implemented based on validation loss to prevent overfitting. This network configuration was optimized through iterative hyperparameter tuning to minimize prediction errors. The finalized FFNN model demonstrated superior performance, achieving the lowest MAE of 15.05 and MSE of 47.65 when compared to other models evaluated.

A perceptron is a type of feed-forward neural network (FFNNs) in which data flows in a straight line from the input layer to the output layer, without coming back again. FFNNs are used for supervised learning; this includes classification and regression. They use activation functions and back-propagation techniques to keep the errors to a minimum, and therefore are appropriate for simple prediction and analysis. Every model has its advantages and, while GANs perform best at generating tasks, FFNNs are more efficient at structured predictive tasks. The workflow of the FS and Htest analysis through ANN starts with the problem definition, followed by objectives that have to be achieved, and the criteria and measures such as mean squared error or accuracy that have to be met. Data collection is then done with the input parameters of material composition and dimensions, and with FS and H test results being the output values obtained(García-Esteban[27]). Subsequently, there is a normalization of the input features and, last but not least, an algorithm that identifies the most influential parameters in the form of either statistical methods or machine learning. To make the evaluation more reliable, the dataset is divided into training, validation, and testing sets. Subsequently, the construction of the ANN model entails designing the layers for input, hidden, and output as the features, the number of hidden layers, and activation functions, such as ReLU, based on the desired prediction output layer. In training, the model fine-tunes itself with the training data set, taking into consideration a loss function like Mean squared Error and an optimizer such as Adam that adjusts weights in cycles. The validation data is used to optimize the hyperparameters and also to avoid overfitting, which is the act of modeling the highs and lows of the training data. After generating the model, this is tested on another dataset, and their efficiency is measured by using tools such as the MAE, MSE, and a coefficient of determination. After the evaluation, Chi-square statistics are used to determine the reliability and accuracy of the model's prediction. There are ways of explaining model behavior and the significance of features, such as feature importance analysis and sensitivity tests. ANN is also used for further purposes such as predicting real-world systems or for implementing testing trials automatically. Last, we compare and contrast experimental values with predicted values to ensure the reliability of the model and elaborate error analysis reports (Vinuja[28]).

The FFNN is then constructed.It has an input layer of nodes equal to the number of features, hidden layers with several neurons and activation functions ReLU, and an output layer with the number of nodes corresponding to the prediction goal. Training the network entails feeding the data into the network and computing an error using a loss function like MSE before getting the weights adjusted using optimization methods such as Adam. After the training session, the model is validated on a different test dataset to assess its performance using measures such as the MAE, MSE, and R-squared. To assess the reliability of the FFNN after the examination of the expectations, its performance is tested for the corresponding values. The role of each supplied input feature is explained with the help of such methods as sensitivity analysis and feature importance. The trained FFNN is then used to solve practical problems by predicting the FS and H values of classes of composites without human input. Last, the results predicted by the model are compared with experimental values, and a comprehensive report is generated that highlights key observations, the errors, and a comparative analysis between the predicted and experimental values (Kibrete[29]).

The GAN model consists of two components: an autoencoder that generates fake signals and a discriminator that decides if the signal is fake or not. While the generator synthesizes reasonable material features to match FS and H values, the discriminator identifies the real and fake data. The GAN is trained for multiple cycles,and the game revolves around the

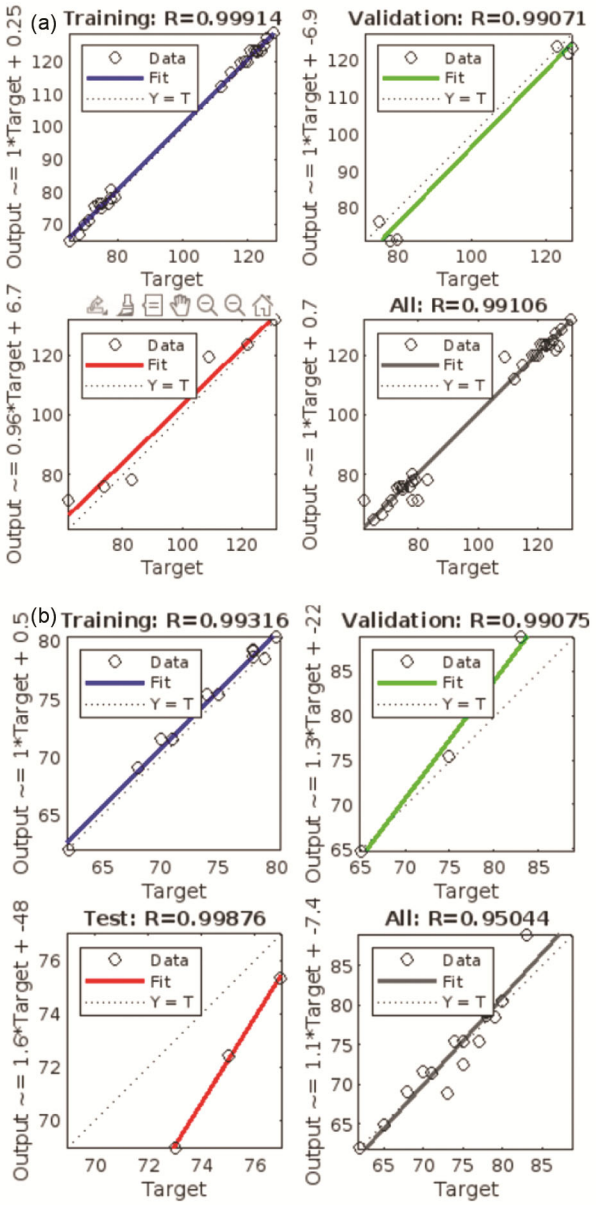


Fig. 14 — Regression plot ANN (a) Flexural and (b)Hardness.

generator and the discriminator, where both have to play to optimize a definite loss function(Wang[30]).

The regression plots in Fig. 14 (a &b) demonstrate the predictive capability of the ANN model in estimating flexural strength and hardness. The Training plot shows an R-value of 0.99914, indicating an almost perfect correlation between the predicted and actual values. The Validation plot has an R-value of 0.99071, confirming that the model generalizes well to unseen data. The Testing plot yields an R-value of 0.985, showing the model's robustness. All-Data plot has an overall R-value of 0.99106, affirming the reliability of the model across all datasets. The

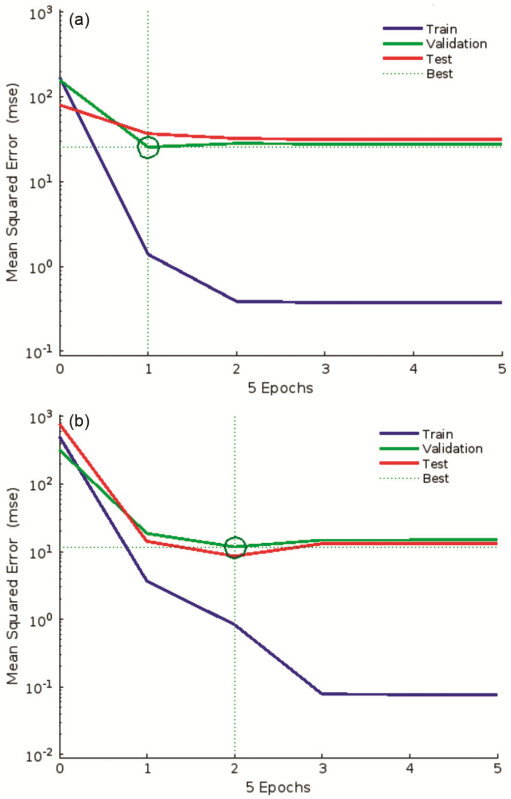


Fig. 15 — Epoch-MSE plot (a) Flexural and (b) Hardness.

Training plot displays an R-value of 0.99316, demonstrating an almost perfect correlation between the predicted and actual values. The Validation plot features an R-value of 0.99075, indicating the model performs well on unseen data. The Testing plot achieves an R-value of 0.9987, reflecting the model's strong robustness. Overall, the All-Data plot has an R-value of 0.9504, confirming the model's consistent reliability across all datasets. Each subplot includes a solid regression line fitted to the ANN output and a dotted Y=T line for reference. The closeness of the two lines indicates that the network output closely approximates the target output. These plots collectively confirm that the ANN model has learned the underlying nonlinear relationships between input features for flexural strength and hardness with minimal deviation.

Figures 15(a&b) present the MSE progression during training, validation, and testing phases of the ANN. The blue curve (training) shows a rapid decline in MSE within the first epoch, demonstrating effective initial learning. The MSE sharply drops from over 100 to below 1 by epoch 2, indicating efficient weight optimization. The green (validation) and red (testing) curves also show quick convergence,

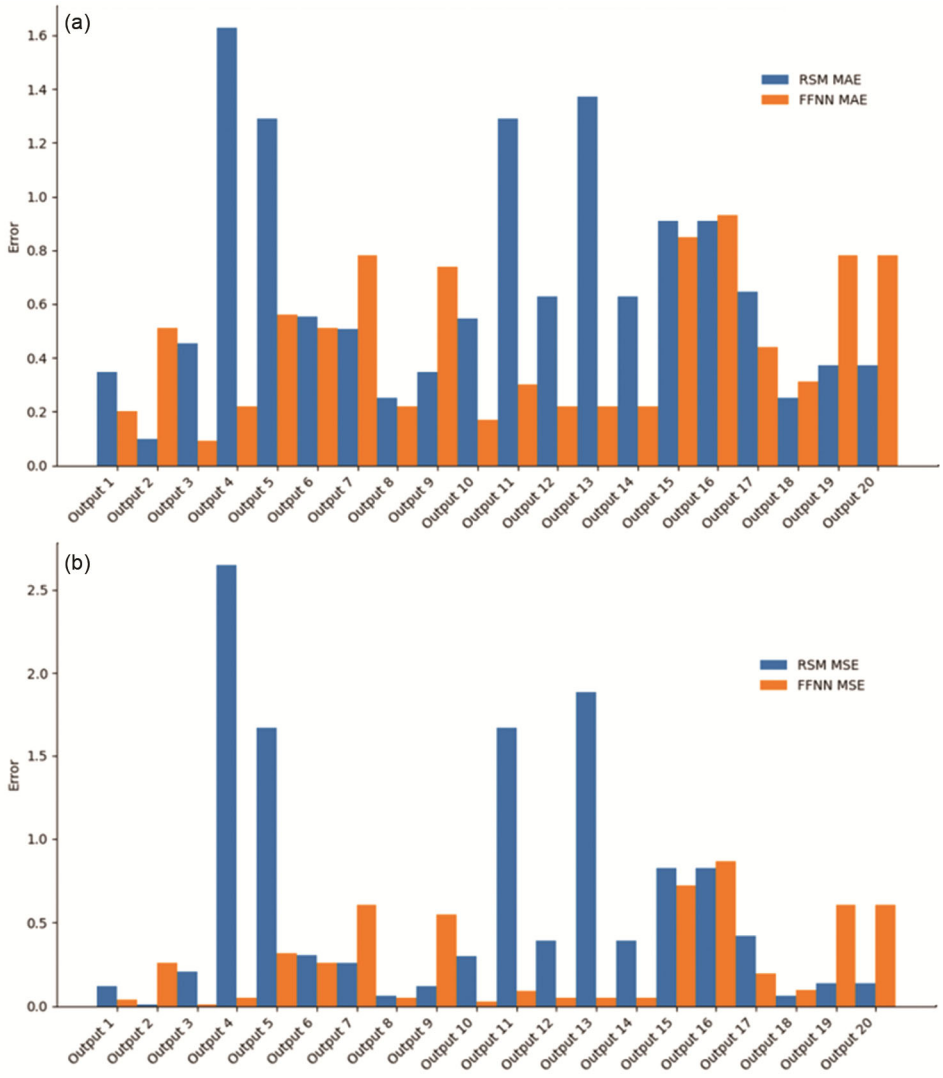


Fig. 16 — Flexural strength (a) MAE plot and (b) MSE plot.

with minor fluctuations, suggesting stable generalization without significant overfitting. The best validation performance is noted at epoch 1, with a minimum MSE of 25.523, as highlighted by the green marker. The log scale used on the Y-axis accentuates the steep decline in error. The convergence of all three curves after early epochs confirms model stability and reliability. Overall, this plot validates the ANN's effective training process and its ability to minimize prediction error quickly while maintaining performance across unseen data.

Figures 16 and 17 compare the performance of two predictive models, RSM and FFNN, in terms of Mean Squared Error (MSE) and Mean Absolute Error (MAE) for various inputs related to FS and H. For FS, the MSE and MAE values indicate that RSM consistently produces higher errors across most inputs, with significant peaks for inputs 4, 11, and 13 Figure 16 (a & b**)**. This suggests that RSM struggles to model the underlying relationships for these inputs effectively. In contrast, FFNN demonstrates lower error values, highlighting its superior capability to capture the complexities of the data. Similarly, for H, RSM exhibits larger errors for inputs like 2, 13, and 14, while FFNN maintains better accuracy with consistently lower MAE values shown in Fig.17 (a & b). The key reason for FFNN's better performance lies in its ability to model non-linear and complex relationships. While RSM relies on quadratic polynomial approximations, which are effective for simpler relationships but limited for highly variable data, FFNN uses a multi-layer architecture and non-linear activation functions. Its optimization process, driven by backpropagation and iterative weight

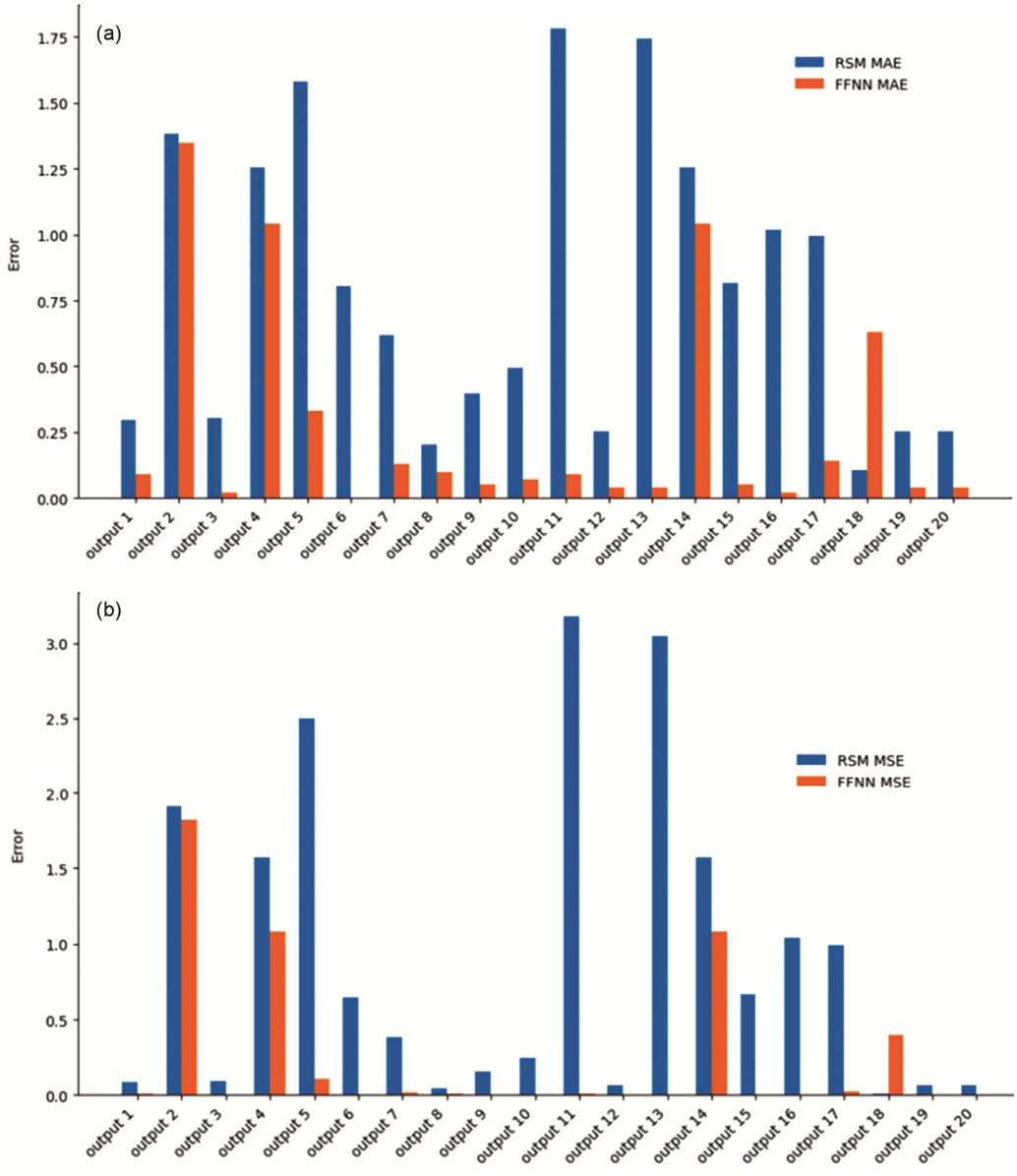


Fig. 17 — Hardness (a) MAE plot and (b) MSE plot.

adjustments, minimizes the loss function (MSE/MAE) during training, enabling the model to generalize well to diverse patterns in the data. On the other hand, RSM's deterministic nature and rigid assumptions about functional relationships restrict its adaptability to complex material properties. FFNN consistently outperforms RSM across all metrics and inputs, proving its robustness and reliability in predicting both FS and H. Its ability to learn and optimize complex relationships makes it a more suitable choice for handling the intricacies of material behavior compared to RSM(Zhou[31]).

The performance metrics depict three models: that are Artificial Neural Networks, Generative Adversarial Networks, and Feedforward Neural Networks, using MAE, MSE, and R^2. Among the models, FFNN gives the lowest MAE (15.05) and MSE (47.65) and the highest R^2 (0.99), demonstrating a better fit for the actual data and thereby giving better predictive accuracy(Rath[32]). For ANN, the MAE is slightly higher (17.05), and the MSE (53.25), but the R^2 value (0.97) is still relatively strong, illustrating that it enhances the ability to determine the latent relationships. In this particular task, the GAN has much higher error values (MAE = 34.47,

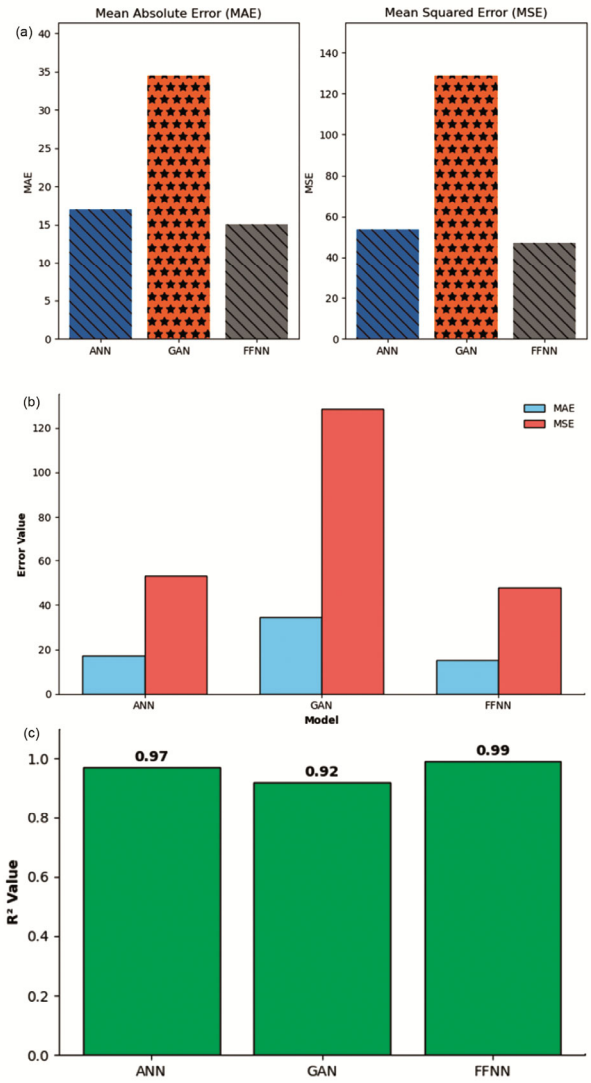


Fig. 18 — (a) Comparison of MSE, and MAE against ANN, GAN, and FFNN, (b) Performance metrics of MSE & MAE and (C) R^2.

MSE = 128.68) and a lower R^2 equal to 0.92. The FFNN is seen to produce the best overall performance shown in Fig.18 (a). FFNN proves to be the overall best mode of estimation, as reflected in its lowest MAE of 15.05, MSE of 47.65, and highest R^2 of 0.99, which demonstrates its superior estimation capabilities. ANN is performed next, yielding a slightly higher MAE (17.05) and MSE (53.25) but a similar R^2 value (0.97) to FFNN. But in this context, GAN performance is relatively poor,as the MAE = 34.47; MSE = 128.68; R^2 = 0.92, as shown in Fig. 18 (b &c),demonstrating that the FFNN can manage the comprehensiveness and variability of the data, depicting it as the most trustworthy model among all the compared models(Zhang[33]).

Figure 19(a) illustrates the comparison of actual and predicted FS for 20 samples using response surface methodology and artificial neural networks. Determination of the FS yields values of 100 to 135 MPa. From the figures indicated it can be noted that both RSM and ANN models have a high regression coefficient, indicating high reliability in estimating mechanical properties. The ANN predictions sometimesoverestimate the real value; this demonstrates the robustness of the model in capturing nonlinear relationships between the variables but can also be overfitting slightly at some times. On the other hand, the RSM predictions are still more predictable, with smaller variations in the negative deviations. The relative consistency between actual and predicted values in most samples validates these predictive models to describe material behaviour(Periyappillai[34]). RSM offers relatively stable and accurate predictions, while ANN is an appropriate approach for capturing more complex patterns; therefore, both can be considered valuable tools for the estimation of FS,with ANN performing better. Figure 19(b) shows the comparative H Prediction plots of the actual and predicted H for 20 samples employing the RSM and ANN approaches. The H values were found on the scale of 60 HRC to 80 HRC, which shows the mechanical properties of the material. The actual measurements are well captured by both RSM and ANN, and this shows the reliability of the models. In some cases, the ANN predictions show slightly higher variances than RSM, with some values crossing the RSM mark, which indicates that it may provide a better fit when distinguishing small fluctuations in data. In contrasts RSM shows a range of similar predictions with less fluctuation. Intriguingly, sample-specific peaks in ANN predictions indicate its capability to learn more intricate material response kinematics(Vinoth[35]). The two methods show the yield of reliable prediction of H and the superior ability of ANN in perceiving the composite and intricate pattern as well as the steadiness of RSM in giving good results, thus establishing that the two methods are useful,but ANN has better prediction against composite materials.A key limitation of this study is the relatively small experimental dataset, which may restrict the model's generalizability. Despite using GANs and regularization techniques, the synthetic data may not fully capture real-world variability. Additionally, the focus on only three parameters may overlook other influential factors affecting composite performance.

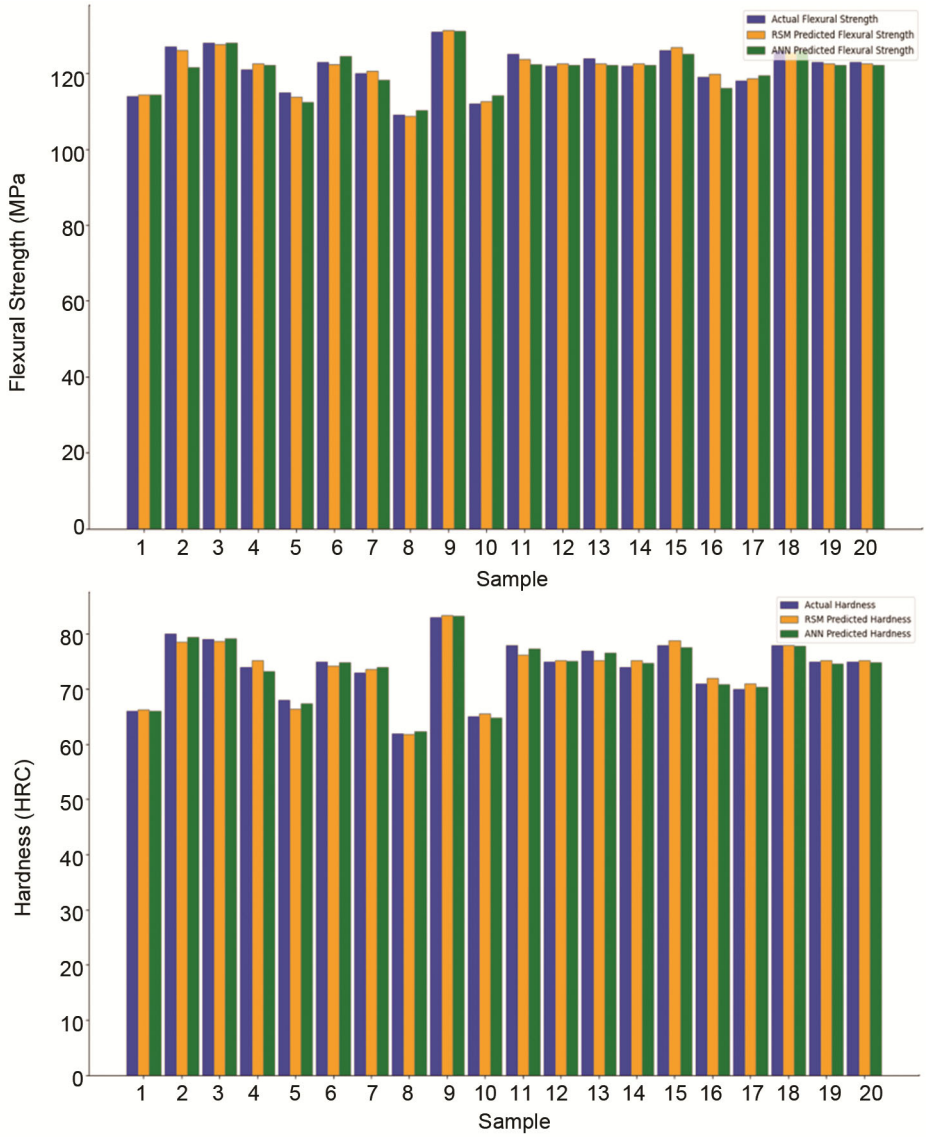


Fig. 19 — (a) Comparison of flexural strength against experimental, RSM & ANN and (b) Comparison of hardness against Experimental, RSM & ANN.

An additional test was conducted using the ANN to further validate the model's predictive accuracy for the studied composite properties. Figure 20 illustrates the relationship between the network's predicted outputs and the actual target values for two different response variables. In each plot, the individual data points (open circles) compare ANN output against corresponding targets, while the solid blue line represents the fit derived from the ANN's predictions and the dotted line denotes the ideal fit where predicted and actual values are equal (Y=T). In Fig.20**,** the flexural plot, the correlation coefficient (R) of 0.97382 demonstrates an excellent agreement between the predicted and actual values, revealing a near-perfect linear relationship and indicating that the ANN effectively captures the underlying data trends for this property. The fit line overlaps closely with the target line, and most data points cluster tightly along this ideal path, further substantiating the model's strong predictive performance. For Hardness shown in Fig. 21, the correlation coefficient (R) of 0.95994 also signals robust prediction accuracy. Although there is a minor departure from the ideal line, the fit remains consistently close, and the majority of data points align well, reflecting the network's reliability even when subjected to data not included during training. These additional test results reinforce the ANN's capability to generalize and accurately predict

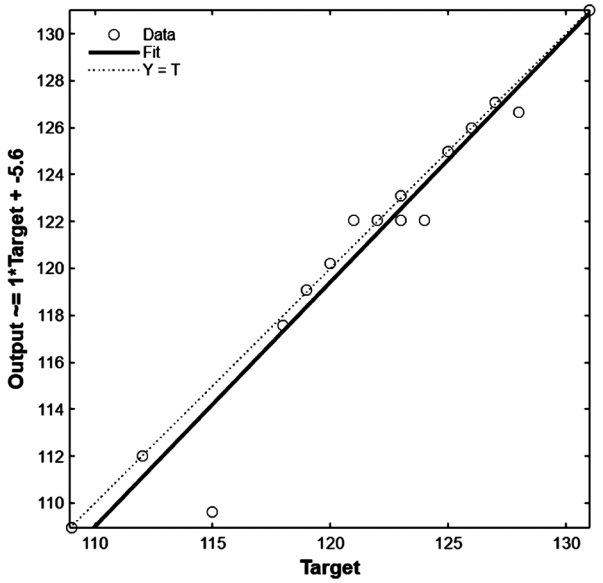


Fig. 20 — Additional test plot for flexural strength.

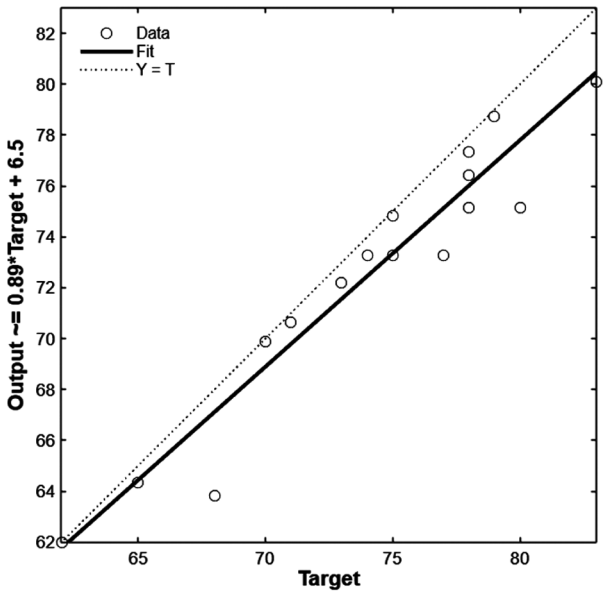


Fig. 21 — Additional test plot for hardness.

outcomes in new, unseen cases. The high R values confirm minimal deviation between model output and actual measurements, supporting the use of ANN as a valid approach for property prediction in composite material optimization. This comprehensive validation builds further confidence in the modelling and data-driven design process.

4 Conclusion

This work studied the flexural characteristics and hardness of hybrid composites containing jute, kenaf, and glass fiber, as well as Al_2O_3 nanoparticle reinforcement. Using RSM, ANN, FFNN, and GAN, the work successfully investigated the interactions between fiber orientation, fiber arrangement, and Al_2O_3 content to predict their impact on composite properties. The experimental observations determined that a 90° fiber angle, the best stacking sequence of G/J/J/K/K/K/K/J/J/G, and 5% Al_2O_3 nanoparticles gave the highest results in flexural strength and hardness. An improvement of 18% in flexural strength and 32% in hardness was observed in the experimental results. This study demonstrated that FFNN outperformed RSM, GAN, and ANN for predicting material properties, indicating the applicability of FFNN for modeling high-order interactions in composites. FFNN was added to the assessment, improving the forecast of the experiment and identifying steady relations between prediction and experiments. The outcome highlighted the effects of fiber orientation, the layering sequence of the individual layers, and the impact of the nanoparticles on the mechanical characteristics of hybrid composites. The utilization of ANN and FFNN enables a forecast of composite performance, which is an excellent advance for expanding the efficiency of material design and minimizing expenditure on experimental iterations. This work highlights the need to have computational methods in close cooperation with experimental models to improve the possibility of sustainable development composites for sustainable use application within the application potential of the developed hybrid composites in high-performance sectors such as automotive, aerospace, and construction, where lightweight, durable, and thermally stable materials are essential. By enhancing flexural strength and hardness through optimized fiber orientation, stacking, and Al_2O_3 nanoparticle reinforcement, these composites serve as strong competitors to conventional materials like carbon fiber and metal alloys, offering a cost-effective and sustainable alternative for structural components.

References

1 Raj M K A, Muthusamy S, Panchal H, Ibrahim A M M, Alsoufi M S & Elsheikh A H, *J Mater Res Technol*, 18 (2022) 3908.
2 Raja T, Devarajan Y, Jayasankar P, Singh D, Subbiah G & Logesh K, *Results Eng*, (2024) 103601.
3 Solairaju J. Arunachalam, Saravanan R & Sathish T, *Results Eng*, 26 (2025) 104523.
4 Velmurugan G, Natrayan L, Chohan J S, Vasanthi P, Angalaeswari S, Pravin P, Kaliappan S & Arunkumar D, *Biomass Convers Biorefin*, 14(20) (2024) 26011.

5 Thanikodi S, Rathinasamy S & Solairaju J A, *Int J Adv Manuf Technol*, (2024) 1.
6 Sekhar S G & Vasudevan A, *Adv Addit Manuf Technol* (2024) 276.
7 Pradeep R, Arumugaprabu V, Geetha P, Sundarakannan R, Vigneshwaran S, Naresh K, Deepak V & Uthayakumar M, *Biomass Convers Biorefin*, 14(17) (2024) 21303.
8 Lakshmaiya N, Vijetha K, Doss A S A, Nitesh K S, Ross N S & Maranan R, *Results Eng*, (2025) 105742.
9 Xian G, Guo R & Li C, *Compos Struct*, 281 (2022) 115060.
10 Aisheh Y I A, Atrushi D S, Akeed M H, Qaidi S & Tayeh B A, *Case Stud Constr Mater*, 17 (2022) e01234.
11 Shah I, Li J, Yang S, Zhang Y & Anwar A, *J Renew Mater*, 10(5) (2022) 1307.
12 Liu C, Hunag X, Wu Y Y, Deng X, Zheng Z & Yang B, *Cem Concr Compos*, 130 (2022) 104508.
13 Sridhar J, Gobinath R & Kırgız M S, *J Nat Fibers*, 20(1) (2023) 2162186.
14 Senthilkumar N, Ramu S & Deepanraj B, *Recent Pat Nanotechnol*, 19(4) (2025) 511.
15 Nwobi-Okoye C C, Anyichie M K & Atuanya C U, *Fibres Polym*, 21 (2020) 898.
16 Ramesh S, M P B H, Gomathi P, Swamy G M, Kandagal Z B & Anne G, *Mater Res Express*, 11(7) (2024) 075302.
17 Arpitha G R, Mohit H, Madhu P & Verma A, *Biomass Convers Biorefin*, 14(11) (2024) 12539.
18 Ramakrishnan S K, Arivendan A & Vijayananth K, *Int J Biol Macromol*, 306 (2025) 141353.
19 Imoisili P E, Makhatha M E & Jen T C, *J Sci Adv Mater Devices*, 9(2) (2024) 100705.
20 Saravanakumar S, Sathiyamurthy S & Vinoth V, *Measurement*, 235 (2024) 114912.
21 Arunachalam S J, Saravanan R, Sathish T & Hourani A O, *2025 8th Int Conf Electron Mater Eng Nano-Technol (IEMENTech)* (2025) 1–6.
22 Nugroho G & Budiyantoro C, *J Compos Sci*, 6(6) (2022) 160.
23 Niyaraki M N, Ghasemi F A, Ghasemi I & Daneahpayeh S, *Tehnički glasnik*, 15(2) (2021) 169.
24 Arunachalam S J, Thanikodi S & Saravanan R, *Results Eng*, 25 (2025) 104571.
25 Arunachalam S J, Saravanan R, Sathish T, Giri J & Barmavatu P, *J Adhes Sci Technol*, 39(2) (2025) 257.
26 Feng F, Ghorbani H & Radwan A E, *Front Environ Sci*, 12 (2024) 1291327.
27 García-Esteban J J, Cuevas J C & Bravo-Abad J, *arXiv preprint*, arXiv:2307.07454 (2023).
28 Vinuja G, Saravanan V, Maharajan K, Jayasudha V & Ramya R, *Emerg Adv AI Big Data Technol Bus Soc* (2024) 128.
29 Kibrete F, Trzepieciński T, Gebremedhen H S & Woldemichael D E, *J Compos Sci*, 7(9) (2023) 364.
30 Wang Y, Soutis C, Ando D, Sutou Y & Narita F, *Eur J Mater*, 2(1) (2022) 117.
31 Zhou Y, Dan M, Shao Y & Zhang Y, *Nano Energy*, 101 (2022) 107586.
32 Rath S, Das N R & Pattanayak B K, *Recent Pat Eng*, 18(2) (2024) 88.
33 Zhang B, Wang S & Ji S, *Ships Offshore Struct*, (2024) 1.
34 Periyappillai G, Sathiyamurthy S & Saravanakumar S, *Fibres Polym*, 25(8) (2024) 3115.
35 Vinoth V, Sathiyamurthy S, Saravanakumar S & Senthil kumar R, *Polym Compos*, 45(7) (2024) 6077.